Ecological Applications, 30(8), 2020, e02204

Unexpected food web responses to low dissolved oxygen in an estuarine fjord

Pamela E. Moriarty,[1] Timothy E. Essington,[1,6] John K. Horne,[1] Julie E. Keister,[2] Lingbo Li,[3] Sandra L. Parker-Stetter,[4] and Mei Sato[5]

[1]*School of Aquatic and Fishery Sciences, University of Washington, Seattle, Washington 98195 USA*
[2]*School of Oceanography, University of Washington, Seattle, Washington 98195 USA*
[3]*Fisheries and Oceans Canada, Delta, British Columbia V3M 6A2 Canada*
[4]*Fishery Resource Analysis and Monitoring Division, Northwest Fisheries Science Center, National Marine Fisheries Service, National Oceanic and Atmospheric Administration, Seattle, Washington 98112 USA*
[5]*Institute for the Oceans and Fisheries, University of British Columbia, Vancouver, British Columbia V6T 1Z4 Canada*

Citation: Moriarty, P. E., T. E. Essington, J. K. Horne, J. E. Keister, L. Li, S. L. Parker-Stetter, and M. Sato. 2020. Unexpected food web responses to low dissolved oxygen in an estuarine fjord. Ecological Applications 30(8):e02204. 10.1002/eap.2204

Abstract. In coastal marine ecosystems, the depletion of dissolved oxygen can cause behavioral and distributional shifts of organisms and thereby alter ecological processes. We used the spatiotemporal variation in the onset and intensity of low dissolved oxygen in Hood Canal, Washington, USA, to investigate consequences of seasonally reduced oxygen on fish–zooplankton predator–prey interactions. By simultaneously monitoring densities of zooplankton (primarily the euphausiid; *Euphausia pacifica*) and zooplanktivorous fish (Pacific herring, *Clupea pallasii*, and Pacific hake, *Merccluccius productus*), and the feeding of zooplanktivorous fish, we could separate the effects of dissolved oxygen on fish–zooplankton interactions from other seasonal changes. We expected that fish predators (especially Pacific herring) would be less abundant and have lower feeding rates when oxygen levels declined below biological thresholds, and that this would result in increased zooplankton abundance in areas with lowest dissolved oxygen. However, these expectations were not borne out. Overall, there was mixed evidence for an effect of dissolved oxygen on many of our response variables, and when effects were detected, they were frequently in the opposite direction of our expectations. Specifically, the pelagic fish community became more abundant (as measured by increasing acoustic backscatter), which was particularly pronounced for Pacific herring. Zooplankton had weak evidence for a response to dissolved oxygen, but the direction was negative instead of positive. Although predator feeding composition was unrelated to dissolved oxygen, stomach fullness (an index of feeding intensity) of Pacific herring declined, as per our expectations. These unexpected findings highlight the importance of in situ measurements of multiple aspects of predator–prey linkages in response to environmental stress to enhance our ability to predict ecological consequences of declining oxygen.

Key words: *crustaceans; ecosystems; estuarine; fishes; food webs/trophic structure; predation.*

Introduction

The large magnitude and rapid pace of global change have generated a high demand for reliable ecological forecasts to aid in planning and to guide policy interventions (Clark et al. 2001). Forecasts of demographic rates, habitat use, and population distributions are often based on generalized laws and relationships derived from macro-ecological principles or data synthesis (Chueng et al. 2013, Deutsch et al. 2015), or from more detailed mechanistic models (Buckley et al. 2010). While such forecasts help identify vulnerable ecosystems and species, predicting how populations or ecosystems will respond to future environmental change is challenging owing to their complexity and adaptation potential (Levin 1998, Walker et al. 2004, Merila and Hendry 2014). Moreover, forecasts must be made with limited understanding of how ecological processes (e.g., predation, competition) will be affected by global change (Harley et al. 2006, Guzzo et al. 2017). Thus, reliable forecasts will benefit from carefully constructed *in situ* observational studies that examine how demographic, behavioral, and physiological responses are manifest in ecological processes.

In coastal marine ecosystems, the frequency, spatial extent, and magnitude of low dissolved oxygen events are increasing (Diaz and Rosenberg 2008, Stramma et al. 2008) due to anthropogenic nutrient loading and

Manuscript received 19 December 2019; revised 1 May 2020; accepted 22 May 2020. Corresponding Editor: Paul K. Dayton.
[6] Corresponding Author. E-mail: essing@uw.edu

warming oceans (Breitburg et al. 2018, Oschlies et al. 2018). The resulting ecological consequences are challenging to predict at a population or ecosystem scale, in part because biological threshold levels that induce lethal or behavioral responses vary depending on the type of biological response (Vaquer-Sunyer and Duarte 2008), are temperature dependent (Pörtner and Knust 2007), and vary widely among species (Deutsch et al. 2015). Nevertheless, a substantial body of work has demonstrated distributional and physiological responses to low dissolved oxygen (where here we define "low" as below species-specific biological thresholds), and that these responses can have ecological consequences. For instance, acute exposure to dissolved oxygen levels beyond physiological limits usually leads to distributional shifts that may alter spatial overlap between predators and prey (Pihl et al. 1991, Breitburg 1992, Eby and Crowder 2002, Craig and Crowder 2005, Ludsin et al. 2009, Zhang et al. 2009).

In pelagic ecosystems, much attention has been paid to how low dissolved oxygen affects the vertical distribution of zooplankton and their predators, and thereby affect the trophic connectivity between them (Ludsin et al. 2009, Pierson et al. 2009, Ekau et al. 2010, Roman et al. 2019). Because of differences in species' tolerance for low dissolved oxygen, the intensity and spatial extent of low dissolved oxygen govern the spatiotemporal overlap of pelagic fish with their zooplankton prey (Keister et al. 2000, Ludsin et al. 2009, Parker-Stetter and Horne 2009, Zhang et al. 2009) and between gelatinous zooplankton and their prey (Decker et al. 2004, Kolesar et al. 2010). Zooplankton may exploit water with dissolved oxygen levels between 1–4 mg/L as predation refugia because they require less dissolved oxygen than their fish predators (Boyd et al. 1980, Stalder and Marcus 1997, Klumb et al. 2004, Vaquer-Sunyer and Duarte 2008).

Low dissolved oxygen can also affect predator–prey linkages in other ways. Low dissolved oxygen affects swimming performance of prey and predators (Domenici et al. 2007) and it alters food intake rates of predators (Nestlerode and Diaz 1998, Pichavant et al. 2001). Finally, the zooplankton community structure (Koslow et al. 2011, Keister and Tuttle 2013, Keister et al. 2020) can be affected by oxygen levels, and thereby alter the availability of preferred prey. Thus, spatial overlap alone may not indicate how predator–prey linkages are altered by exposure to dissolved oxygen below biological thresholds.

Here, we examine how low dissolved oxygen affects the trophic connectivity of zooplankton and their fish predators in an estuarine fjord. Hood Canal, Washington (USA) is naturally prone to low dissolved oxygen, particularly in the southern areas because of limited exchange with the Pacific Ocean. Consequently, there are sharp spatial and seasonal differences in oxygen concentrations, which we exploit to evaluate how dissolved oxygen levels affect pelagic fish, their zooplankton prey, and predation linkages between them. Earlier work documented little change in predator–prey overlap, despite dissolved oxygen levels near 2 mg/L (Sato et al. 2016). The present work extends that analysis by exploring responses of metrics relevant for food web connectivity (predator and prey densities, predator feeding rates, and diet composition) within a single statistical framework.

We adopt a multi-model inference approach to judge the weight of evidence that dissolved oxygen affected zooplankton and their main fish predators. Rather than a priori specifying the threshold levels of dissolved oxygen where we expect biological responses, we instead develop and apply a statistical model to estimate these thresholds directly from the data, while also accounting for uncertainty in this threshold when estimating the effect of dissolved oxygen on this pelagic food web. We hypothesized that predator feeding rates and densities would decline as oxygen declined below thresholds. We hypothesized that this effect would be strongest for Pacific herring, *Clupea pallasii,* which generally inhabits mid water column pelagic habitats, and weakest or non-existent for Pacific hake, *Merluccius productus*, which commonly inhabit deep, poorly oxygenated waters (<2 mg/L) along the Northeast Pacific continental shelf (Keller et al. 2010). Finally, we hypothesized that these responses would weaken predation intensity on zooplankton prey, resulting in increased zooplankton densities when oxygen was below thresholds.

Methods

Sample site

Hood Canal (Fig. 1) is an estuarine fjord that constitutes the western branch of Puget Sound, Washington, USA. Hood Canal is an ideal study system to test our hypotheses because it contains large spatial contrasts in the timing and intensity of oxygen depletion across regions that otherwise share many environmental characteristics. In the northern regions of Hood Canal, relatively high oxygen concentrations (>5 mg/L) are maintained by periodic intrusions of coastal water (Babson et al. 2006, Sutherland et al. 2011). Because this replenishing water typically does not reach the southern Canal, dissolved oxygen concentrations decline seasonally and hypoxic water extends upward to 20–30 m below the surface by late summer or fall (Newton et al. 2007). By late October, weakened stratification typically permits mixing and restoration of oxygen to depleted waters. Unlike some estuarine ecosystems, Hood Canal does not have extensive freshwater inputs so salinity gradients are small. This spatial patterning of hypoxia across short distances, combined with similarities in other environmental characteristics across sites, provided us a unique opportunity to use inter-site comparisons to test the effects of hypoxia. For a summary of seasonal and long-term temporal trends in dissolved

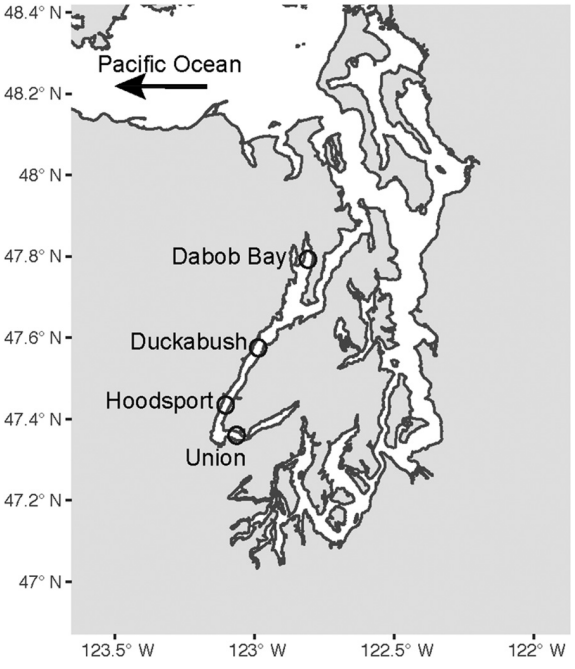

FIG. 1. Map of Puget Sound, Washington, USA showing the location of each sampling site in Hood Canal.

oxygen conditions, see Newton et al. (2007) and Brandenberger et al. (2011).

Sampling design

We monitored four sites within Hood Canal through time to distinguish the effects of dissolved oxygen from local characteristics of sampling sites and other biological and environmental phenology. Two sampling sites (Union and Hoodsport) were located at the southern end of Hood Canal where dissolved oxygen typically becomes hypoxic toward the end of summer. A second pair of sampling sites (Duckabush and Dabob Bay) were located in the northern region where oxygen levels usually remain higher (Fig. 1). Sites were selected to create pairs with similar bathymetry: Union/Dabob Bay, and Hoodsport/Duckabush share similar bottom depth profiles, although we do not directly match sites in our statistical analysis. We sampled monthly from early June to early October in 2012 and 2013 for a total of five sampling periods each year. Our goal was to monitor the system before, during, and after the onset of seasonal low (e.g., 2–4 mg/L) dissolved oxygen. As fish feeding and zooplankton spatial distributions are known to have diel patterns, we sampled during the day and night at each station during each sampling period. Hereafter, sampling variables will be referred to as site, year, month, and diel, and a sampling event refers to a single site–year–month–diel combination.

Temperature and oxygen sampling

To characterize the temperature and dissolved oxygen profiles of the water column, we performed 1- 4 Conductivity-Temperature-Depth (CTD) casts per site (usually one in the day and one at night) using a Sea-Bird Electronics SBE 911plus equipped with a Niskin rosette and an SBE 43 dissolved oxygen sensor (Bellevue, Washington, USA). The sensors were annually calibrated by Sea-Bird and calibrated during field surveys with oxygen titrations conducted following the modified Winkler Method (Carpenter 1965). The data were processed into 1-m depth bins then averaged across all replicate casts; environmental conditions were assumed to be horizontally uniform within each site. These data were used in statistical modeling to link dissolved oxygen levels to biological responses (see "Statistical Analysis").

Acoustic surveys

We measured acoustic backscatter along transects within each site to assess densities of pelagic fish and zooplankton. Acoustic backscatter data were obtained using Simrad EK60 splitbeam echosounders (Kongsberg Maritime, Kongsberg, Norwary) operating at 38, 70, 120, and 200 kHz as described in Sato et al. (2016). All transducers were deployed on a pole mounted on the side of the boat at 2 m below the surface. The 70, 120, and 200-kHz transducers had beam widths of 7° while the 38-kHz transducer had a beam width of 12°. The echosounders sampled at a frequency of 0.5–2.0 pings/s with a pulse duration of 512 μs. At each site, acoustic backscatter (i.e., reflected energy) measurements were taken over a fixed grid of six to eight parallel transects spaced 500 m apart at a boat speed of five to six knots (1 knot = 1.85 km/h). The same grid was sampled during each sampling event at a site.

Zooplankton sampling

Zooplankton community composition was determined using a five net Hydro-Bios MultiNet system (Altenholz, Germany) with a 0.25-m^2 mouth opening, equipped with 335-μm mesh nets, double flow meters, and a CTD sensor. Depth-stratified tows were conducted within the survey areas at a speed of 1–2 m/s, spending 1–7 minutes in each depth layer depending on its thickness. Target sample depths were chosen based on backscatter densities observed on the echosounder conducted immediately prior to net tows; hereafter these are termed "acoustic layers." Typically, two acoustic layers were sampled for each sampling event. Where no clear layers were observed, a net tow was conducted over the full water column. All samples were preserved in 5% formalin in buffered seawater and returned to the laboratory for analysis.

Fish sampling

We used midwater trawls to assess the fish community composition and to collect samples for quantifying fish

feeding habits. A Marinovich midwater trawl with a 3.2-mm knotless liner in the codend was towed at a boat speed of 1.7–5.5 km/h and outfitted with a real-time pressure sensor (PI50, Kongsberg Maritime). The vertical opening of the trawl net ranged from 4.8 **to** 7.0 m. Typically, we aimed to conduct two trawls at each sampling event, though the actual number of trawls varied from one to four, for a total of 149 trawls. Trawl duration varied from 3 to 33 minutes depending on observed acoustic backscatter (longer when lower backscatter), but typically lasted for 8 minutes. Trawl depths were chosen to representatively sample the spatial distributions of acoustic backscatter at each site, while also targeting depths where fish were most dense. During our study, zooplanktivorous fish were mainly comprised of Pacific herring and Pacific hake (Sato et al. 2015, 2016), which together accounted for 82−100% of total sampled fish biomass at Dabob, 53–100% at Duckabush, 84−100% at Hoodsport, and 82−100% at Union. We therefore focused our analyses on these two species. Often, we performed one trawl tow through a dense backscatter layer (typically hake) and a second that targeted discrete fish aggregations (typically herring).

Following capture, fish were separated by species, then each species' catch was counted and weighed using a digital scale. When abundance exceeded roughly 15 kg, total abundance was estimated by subsampling a weighed portion of the total catch. For each trawl sample, we randomly selected 100 individuals of each species to measure total lengths; when fewer than 100 were captured, we measured all individuals.

To collect information on fish feeding habits, we collected up to 50 herring stomachs and 50 hake stomachs from the trawls for each sample. Individual total lengths (mm) of the fish were measured, and stomachs were removed from the individuals and preserved in 90% ethanol. We evenly divided stomach samples among tows to the extent possible.

Processing and analysis of samples and data

Acoustics.—Acoustic data were processed using Echoview (version 5.4; Echoview Software Pty Ltd, https://www.echoview.com/). Vessel noise estimated during acoustic surveys was removed by linear subtraction. Data shallower than 5 m depth were removed from analyses to eliminate near-field transducer effects and surface bubbles. Similarly, data within 0.5 m of the echosounder-detected bottom were removed.

The nautical area scattering coefficient (NASC; m^2/nautical $mile^2$ [1 nautical mile = 1.85 km]; Maclennan et al. 2002) was calculated for all backscatter measurements along each transect at each site. This metric integrates backscatter through the water column and standardizes area to a square nautical mile. NASC values from each transect were then averaged for each sampling period and site.

We classified total acoustic backscattering strength (Sv, dB re 1 m^{-1}; Maclennan et al. 2002) to taxonomic groups by applying the classification procedure defined by Sato et al (2015). Briefly, this method uses backscattering frequency responses to classify backscatter as either zooplankton or fish (hereafter referred to as combined fish). For day samples, combined fish was further classified as Pacific hake or Pacific herring based on distribution morphologies. This species-level classification was not possible during night samples because of high spatial overlap in herring and hake distributions and a lack of species-specific characteristic schooling patterns (Sato et al. 2015).

Because euphausiids were the primary prey of both herring and hake (see methods subsection *Fish*), we sought to determine how much of the zooplankton-classified backscatter was attributed to euphausiids. To this end, we used MultiNet zooplankton samples to calculate the numerical proportion of zooplankton that were euphausiids (p_{euph}). In the MultiNet samples, copepods were the most numerically dominant species (averaging 67%), while euphausiid juveniles and adults comprised 0.3–28% of the numerical percentage (averaging 9.3%). We averaged MultiNet samples collected at the same sampling event when needed, weighting each MultiNet catch by the depth range sampled. We then estimated the proportion of NASC attributable to euphausiids from the ratio, R, of Sv produced by individual euphausiids to copepods at 200 kHz from Fig. 1b in Lavery et al. (2007). Assuming that all other zooplankton species produce similar backscatter as copepods, the proportion of NASC attributable to euphausiids equals

$$p_{\text{NASC}} = \frac{Rp_{\text{euph}}}{Rp_{\text{euph}} + (1 - p_{\text{euph}})} \quad (1)$$

where $R = 116$. The derivation of Eq. 1 appears in Appendix S1.

Euphausiids accounted for >85% of the NASC for more than 70% of the samples (Appendix S1 Fig. S1). Exceptions occurred when total backscatter was relatively low (e.g., <50 m^2/nmi^2). We concluded therefore that zooplankton NASC serves as a useful proxy for euphausiid abundance.

Zooplankton.—Subsamples of all collected zooplankton were identified to taxonomic group, counted, and measured using the silhouette method (Davis and Wiebe 1985, Little and Copley 2003). Body length of 30–500 individual euphausiids from each MultiNet tow was measured from the posterior base of the eye stalk to the end of the sixth abdominal segment (Mauchline 1980). For all other taxa, total length was measured. These measurements were used to convert counts to biomass using previously derived length–weight relationships (Williams and Robins 1979, Webber and Roff 1995, Lavaniegos and Ohman 2007). Both predator species exhibited strong size selectivity for euphausiids (see methods subsection *Fish*), so we additionally estimated

the fraction of sampled euphausiid biomass that was from individuals ≥ 10 mm. For each tow, a kernel density smoother was fit to the empirical length distribution and the fitted kernel density was used to estimate the proportion of euphausiid biomass derived from ≥ 10 mm individuals.

Fish.—To analyze individual fish feeding, each fish stomach was dissected and the total stomach content was weighed to the nearest 0.1 g. Contents were separated by taxonomic group and each group was weighed and counted. Contents that were too digested to identify were classified as "unknown." We aimed to process 25 stomachs of each species per trawl, selected randomly from the fish collected. When fewer than 25 of a species were caught in a trawl set (which occurred five times for herring and nine times for hake), all stomachs were processed from that sample. The numbers of stomachs collected and processed by sampling event and species are provided in Appendix S1: Table S2.

We determined the size selectivity of herring and hake predation on euphausiids by measuring lengths of individual euphausiids in a randomly chosen subset of fish stomachs under a dissecting microscope. For the first 1,000 intact euphausiids measured across all stomachs analyzed, we measured both carapace length and body length to estimate the ratio between them, and applied this ratio to estimate body length when only carapace length could be measured. Euphausiid lengths were measured for each fish species for each month for a total of 898 euphausiids from hake stomachs and 1,369 euphausiids from herring stomachs. For both species, the lower quartile was approximately 10 mm, so we used this cutoff value to define the fraction of euphausiids that were "large" in the statistical analyses.

We standardized stomach fullness by dividing the observed stomach mass by a value that is approximately proportional to fish total mass. Presuming that fish weight scales with body length to the power of 3, then stomach content mass/(fish length)^3 is a metric of stomach fullness that is comparable across different-sized fish.

The fraction of diet (by mass) consisting of euphausiids was calculated using the estimation model of Moriarty et al. (2017): this model accounts for potential covariance between diet composition and feeding rate and is robust to outliers. We created a Bayesian version of this model, which provided more robust estimates of observation error and variance. Details of the model and implementation are provided in Appendix S1

Statistical analysis

We assessed the effect of dissolved oxygen concentration on feeding (stomach fullness, diet composition), fish backscatter, and zooplankton backscatter by fitting multiple statistical models, and evaluating the degree of support for each alternative model. We fit models in a Bayesian framework, where site was modeled as a random effect to account for the lack of independence among samples collected in the same site (Gelman 2006), and to account for the environmental conditions unique to each site. We chose a Bayesian framework because of the computational ease of fitting multi-level nonlinear models.

A non-linear model was used to incorporate potential effects of oxygen concentrations on ecological response metrics and to estimate the threshold oxygen concentrations. Because oxygen is a limiting factor in metabolism (Fry 1971, Deutsch et al. 2015), we expected no effect of dissolved oxygen above some threshold and increasing effects of dissolved oxygen below this threshold (Pollock et al. 2007). Fitting this model required that we characterize dissolved oxygen concentrations throughout the water column using a single metric. We chose the average dissolved oxygen concentration at depths greater than 20 m as our index of water quality. This depth range was chosen for three reasons. One, it is consistently below the mixed layer, so it is not subject to variability arising from surface mixing and phytoplankton blooms (Appendix S1: Figs. S3, S4). Two, it is the depth range used previously to summarize trends in water quality conditions in Hood Canal (Newton et al. 2007). Three, 90% of our midwater trawl tows were deeper than this depth. Thus, this metric is a useful indicator of the extent and intensity of dissolved oxygen conditions relevant for pelagic food web linkages measured in this study. Standard errors of mean dissolved oxygen for individual CTD casts were calculated using the method described by Flyvbjerg and Petersen (1989), as described in Appendix S1.

We used a weight of evidence approach to judge support of our hypotheses, which is more appropriate for environmental impact assessment than null hypothesis testing (Hilborn and Mangel 1997, Anderson et al. 2000). To that end, we fit several alternative models and evaluated the weight of evidence for each. All models included multi-level effects of sampling site and fixed effects for time of day (when appropriate) and year. For backscatter metrics, we additionally considered all possible combination of models that included month (to account for phenology unrelated to dissolved oxygen), and dissolved oxygen (mean dissolved oxygen at depths > 20 m). For feeding metrics, we also considered models that included as predictors the proportion of sampled euphuasiids that were large, i.e., exceeded 10 mm in length (Appendix S1: Fig. S2).

All alternative models took the form

$$\mathbf{y} = \mathbf{X}\boldsymbol{\beta} + \mathbf{Z}\mathbf{u} + \epsilon \tag{2}$$

where $\mathbf{y}$ is a vector of observations (the response variable), $\mathbf{X}$ is the model matrix for fixed effects, $\mathbf{Z}$ is the model matrix for site effects, $\boldsymbol{\beta}$ and $\mathbf{u}$ are vectors of fixed effect and random effect coefficients, respectively, and $\boldsymbol{\varepsilon}$ is a vector of residuals, assumed to be normally

distributed with mean of 0 and standard deviation σ. For diet composition and diet fullness, we included estimated sampling error (σ_{obs}) because sample sizes and precision varied, so that the total standard deviation of equaled

$$\sigma = \sqrt{\sigma^2_{\text{model}} + \sigma^2_{\text{obs}}} \quad (3)$$

The multi-level parameters (i.e., site effects) were assumed to follow a normal distribution with mean equal to μ_u and standard deviation σ_u. Data were transformed as needed to be approximately normal: diet fraction was logit transformed while all other variables were $\log_e$-transformed.

To allow for nonlinear effects of oxygen concentration, the fixed effects matrix **X** was modified (**X***) within the estimation procedure. We sought to estimate both the effect (slope) of dissolved oxygen, and the threshold above which dissolved oxygen had no effect. We defined the *j*th column of **X** as the column containing the measured average dissolved oxygen concentration. For all columns other than *j*, **X*** equaled the corresponding column of **X**. For the *j*th column

$$\mathbf{X}^*_{ij} = \begin{cases} \mathbf{X}_{ij} - X_{\text{threshold}} & \text{if } \mathbf{X}_{ij} \le X_{\text{threshold}} \\ 0 & \text{otherwise} \end{cases} \quad (4)$$

where *i* indexes observation. Fixed effects on the response variable were then calculated from the product of **X***β. All response variables were standardized to have a mean equal to 0 prior to model fitting.

We used weakly informative priors on parameters to aid in model convergence. Cauchy priors were used for $\beta_{i,j}$ with location and scale parameters set to 0 and 2.5 (Gelman 2006). A location parameter of 0 represents a prior belief that there were roughly equal odds of a positive or negative effect of each predictor. A scale parameter of 2.5 means that a coefficient of 2.5 was presumed to be one-half as likely as a coefficient of 0, i.e., this was a very broad prior that had little influence on the posterior probability distribution. Priors for site effects were also weak, so that ~μ_μ Cauchy (0, 2.5). We used half Cauchy priors for all parameters (Gelman 2006), with location set to 0, where σ_{model} had its scale parameter set to 2.5 and σ_u set to 1. The more restricted prior for σ_u was necessary because convergence issues arose when it was less constrained. We used a skew normal prior between 2.0 and 8.0 mg/L dissolved oxygen for $X_{\text{threshold}}$, where the location parameter equaled 5, scale parameter equaled 10, and the slant parameter equaled −10. This produced a moderately informative prior, such that there were relatively similar prior densities between 2 and 4 mg/L, and declining prior probability at higher dissolved oxygen levels that approached zero density near 8 mg/L (Appendix S1: Fig. S2). This captured our prior belief that the biological threshold was unlikely to exceed 5–6 mg/L (Vaquer-Sunyer and Duarte 2008). We set the lower limit at 2.0 mg/L because this was near the lower limit of our dissolved oxygen data.

Parameters were estimated numerically using Markov Chain Monte Carlo methods, using Stan (Stan Development Team 2017) with the NUTS (no u-turn sampling) algorithm (Carpenter et al. 1998, Hoffman and Gelman 2014, Stan Development Team 2017) and rstan v. 2.15.1 (Stan Development Team 2017), run in R v 3.5.1 (R Development Core Team, 2017). Models were run with three chains of 2,500 iterations each, plus a warm-up period of 2,500 iterations, which is generally sufficient for the NUTS algorithm (Vehtari et al. 2017). Chains were not thinned because autocorrelation was not detected. Model outputs were checked to ensure few divergent transitions occurred, and that convergence was evaluated based on the scale reduction factor $\hat{R}$ (Gelman and Rubin 1992). Posterior predictive checks were visually analyzed to evaluate model fit.

We used Bayesian model weights to judge the degree of support for each model. Briefly, this procedure involves first using leave-one-out cross-validation to calculate the predictive ability of each model. Leave-one-out cross-validation means fitting a model to all data points but one (denoted y_{-i}, meaning the set of data minus data point *i*), generating a prediction for the excluded point y_i, and then evaluating the predictive probability density of the point, given the model prediction for that point. For instance, if a model predicts a mean value $\hat{y}$, and a standard deviation σ, the model's predictive probability density of y_i is $N(y_i|\hat{y}, \sigma)$. Because this is a Bayesian model, there are many different mean values and standard deviations, so we calculate the expected predictive probability density, which we denote $E(p(y_i|y_{-i}))$.

Bayesian model weights for each of the *k* models (w_k) are then calculated using the stacking method (Yao et al. 2018), which maximizes the (log) weighted sum of predictive densities over all models

$$\max_{w \in S_1^K} \frac{1}{n} \sum_i^n \log \sum_{k=1}^K w_k E(p(y_i|y_{-i}))_k \quad (5)$$

where the notation S_1^K indicates constraints on the model weights so that that each model weight is bounded between 0 and 1, and the sum of weights equals 1. Models with higher model weights have greater support. The calculation of leave-one-out predictive distributions can be computationally expensive, as it requires fitting the model *n* times (where *n* is the sample size). We used the efficient approximation method provided by Vehtari et al. (2017), which uses Pareto-smoothed importance sampling to estimate the expected log point density using the Markov Chain Monte Carlo output fit to the full data.

To be consistent with commonly used information criteria (BIC, WAIC, AIC), we also calculated the LOOIC (leave-one-out information criterion), which can be interpreted in similar ways. We used the loo() package (v

2.2.0) to estimate expected log point density, LOOIC, and the model weights (Vehtari et al. 2019).

We also sought to examine the estimated direction and magnitude of effect sizes to see if estimated changes were consistent with our expectations. To that end, we defined the effect size for each response variable as the difference between the predicted value of a response variable when mean water column oxygen equaled 2.0 mg/L compared to the predicted value when mean water column oxygen exceeded the estimated dissolved oxygen threshold. We used dissolved oxygen = 2 mg/L because this value is commonly used as a threshold defining hypoxic conditions, and was near the lowest value of average dissolved oxygen we observed. For all variables except for diet fraction, these effect sizes are log response ratios (because the response variable was log-transformed). For diet fraction, these effect sizes were odds ratios. Because more than one of the alternative models contained dissolved oxygen as a predictor, we presented the posterior probability distribution from whichever of these models had the strongest evidence, based on Bayesian model weight.

Results

First, we describe observed temporal and spatial patterns in dissolved oxygen and the response variables, and then report on results of statistical model fitting.

Summary of dissolved oxygen

As expected, our index of water quality (mean water column dissolved oxygen concentrations) varied across sampling sites and sampling months (Fig. 2). In 2012, mean dissolved oxygen concentrations were relatively high (~5 mg/L) in June, and declined steadily thereafter. Mean dissolved oxygen was lowest in October at the Union and Hoodsport sites. In 2013, spatial differences were similar to 2012 but the seasonal cycle appeared different (Fig. 2). Both Union and Hoodsport had lower initial dissolved oxygen concentration in June (<4 mg/L), and reached the lowest levels in August (Hoodsport) or September (Union). Mean dissolved oxygen concentrations increased in October in the two southern sites to levels similar to those observed in June 2013. These inter-annual differences in the seasonality of water quality were fortuitous because it allowed us to better separate the effects of dissolved oxygen from those due to biological phenology. Generally, dissolved oxygen concentrations at a site varied only slightly from 20 m to the bottom (Appendix S1: Fig. S3). Southern sites were occasionally 1°–1.5°C cooler than northern sites (Appendix S1: Fig. S4).

Summary of response variables

Zooplankton backscatter exhibited diel, seasonal, and inter-annual patterns (Fig. 3). For most sites, backscatter was greatest during daytime. In 2012, there was little apparent seasonality in zooplankton backscatter, and the two southern sampling sites (Union and Hoodsport) usually had the highest observed backscatter. In 2013, there was a more pronounced seasonal pattern in zooplankton backscatter, with backscatter increasingly slightly throughout the sampling period. The Union site had the lowest backscatter in 2013, but commonly the highest in 2012.

Both herring and hake fed predominantly on euphausiids, with diet fractions commonly exceeding 50%. There was a tendency, particularly for herring, to have higher euphausiid diet fractions in September and October (Fig. 4). Increased preference for euphausiids likely reflects the predator's preference for large euphausiids, which were more common in late summer and early autumn (Appendix S1: Fig. S5). Stomach fullness (Appendix S1: Fig. S6) did not show clear patterns across sites, years, or seasons. Herring and hake acoustic backscatter also did not show clear patterns across sites, years, or seasons (Appendix S1: Fig. S7).

Statistical analysis

The weight of evidence in support of models with dissolved oxygen as a predictor varied among the response variables. Among the backscatter metrics, zooplankton had the least weight of evidence for a dissolved oxygen effect, with nearly 85% of the weight given to the base model (only site, year, and diel period as predictor variables), and the remaining 15% was given to the model containing site, year, diel period, month and dissolved oxygen (Table 1). There was greater evidence for dissolved oxygen affecting the three fish backscatter metrics. For combined fish and for Pacific hake, nearly two-thirds of the model weights were given to the model containing both the base predictors and dissolved oxygen (Table 1). For Pacific herring, all of the model weight was assigned to the model containing base predictors and dissolved oxygen (Table 1). These model weights were consistent with the LOOIC model selection criteria (Appendix S1: Table S3).

There was less evidence that dissolved oxygen affected the feeding metrics. For Pacific hake diet fraction and stomach fullness, all of the models containing dissolved oxygen had 0% weight (Table 2). Instead, these metrics were more strongly associated with seasonality (month) and the fraction of euphausiids that were larger than 10 mm, while the base model had roughly 30% model weight. There was also little evidence in support of a dissolved oxygen effect on Pacific herring diet fraction: the model weights were shared between two models that described temporal changes in euphausiid size composition, either with (58%) or without (42%) month (Table 2). There was more support for dissolved oxygen affecting Pacific herring stomach fullness, as nearly three-quarters of the model weight was assigned to the model containing the base predictors, the fraction of

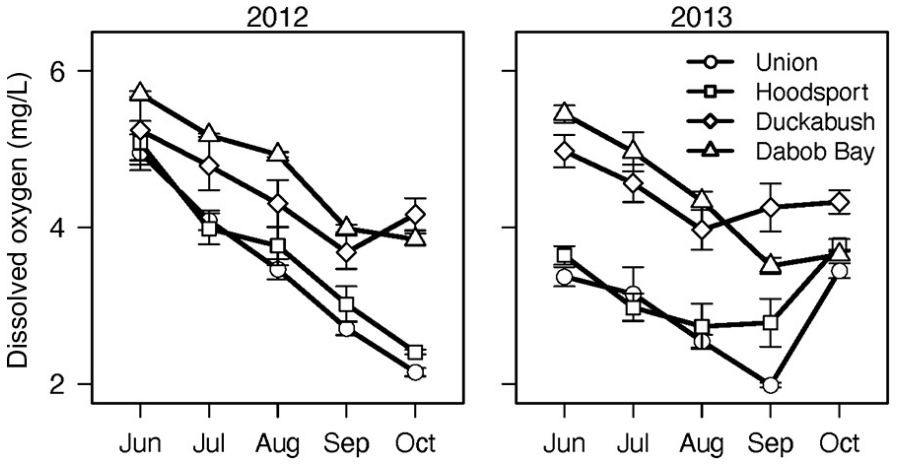

FIG. 2. Dissolved oxygen (mean ± SE) by month, year, and sampling site. Data are averages of replicate casts of the dissolved oxygen sensor at each site, where dissolved oxygen was averaged over depths > 20 m.

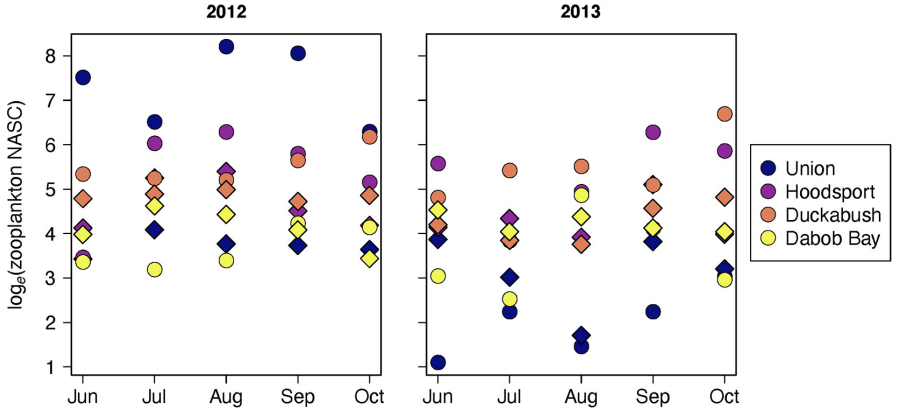

FIG. 3. Seasonal patterns of zooplankton backscatter in 2012 (left) and 2013 (right). Circles denote day samples, diamonds denote night samples. NASC, nautical area scattering coefficient. [Color figure can be viewed at wileyonlinelibrary.com]

euphausiids that were large, and dissolved oxygen (Table 2).

The posterior densities of estimated effect sizes were evaluated to determine the sign and direction of effects. For zooplankton backscatter, the estimated effect size for dissolved oxygen (Fig. 5) was more likely to be negative than positive, contrary to our expectation. We note that this model was not well supported by model selection (Table 1), and the 80% credible interval included 0. For fish predators, the findings were mixed. For combined fish and for Pacific herring, reductions in dissolved oxygen below the estimated thresholds led to increases in backscatter (Fig. 5), and the 80% credible intervals did not include 0. The effect size was particularly large for Pacific herring, where the median log response ratio was near 1, but was smaller (near 0.5) for combined fish. These responses were in the opposite direction of our predictions. For Pacific hake the reverse was true: reductions in dissolved oxygen below the estimated threshold led to a decline in herring backscatter (Fig. 5), and the 80% credibility interval did not contain 0. The posterior probability distributions of effect sizes for feeding metrics tended to be broad and span 0, consistent with the model weights indicating little support for an effect of dissolved oxygen (Fig. 6). However, the analysis indicated a higher probability that Pacific herring stomach fullness declined as dissolved oxygen declined below the estimated threshold (Fig. 6).

The dissolved oxygen thresholds were not precisely estimated (Table 3), but there were some notable differences among response variables. When model selection gave little support for an effect of dissolved oxygen on a response variable, the estimated posterior distributions of dissolved oxygen thresholds were roughly similar to the prior distribution (Table 3). Effects on Pacific hake backscatter were estimated to occur at the lowest dissolved oxygen levels (80% credible interval = 2.2–3.3 mg/L), while effects on Pacific herring stomach

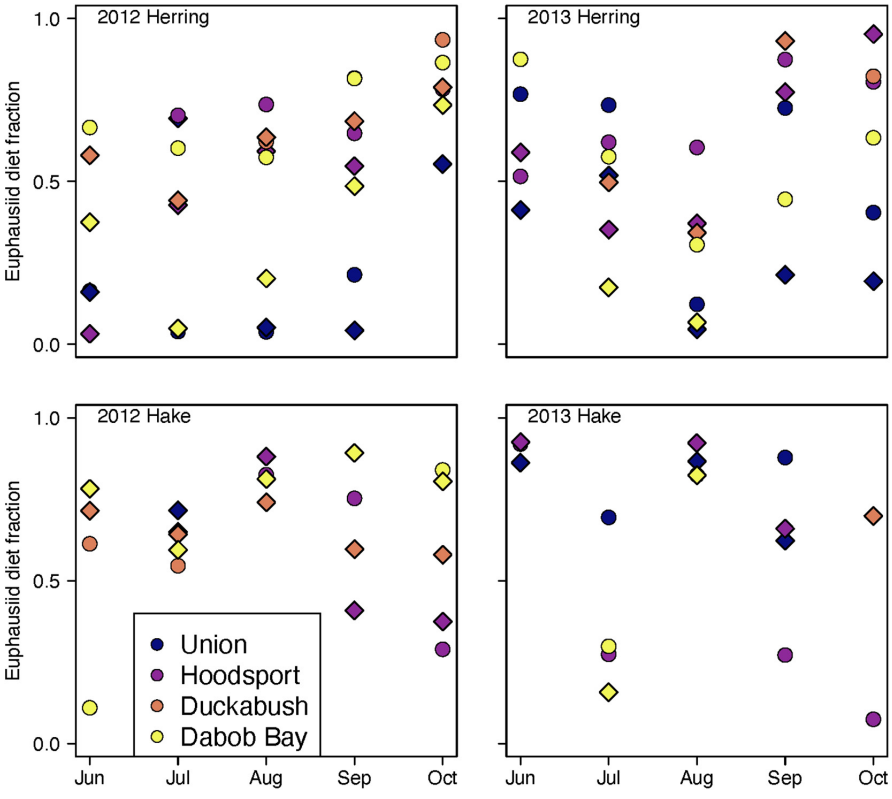

FIG. 4. Seasonal trends in the fraction of herring (top) and hake (bottom) diet contents that consisted of euphausiids. Symbol color denotes sampling site. Circles denote day samples, diamonds denote night samples. [Color figure can be viewed at wileyonlinelibrary.com]

TABLE 1. Model weights for alternative models for each backscatter response metric.

Model	Zooplankton	Combined fish	Pacific herring	Pacific hake
Base	0.848	0	0	0.335
Base + Month	0	0.319	0	0
Base + Dissolved Oxygen	0	0.681	1	0.665
Base + Dissolved Oxygen + Month	0.152	0	0	0

Notes: Base refers to the combination of Site random effects and Year + Diel fixed effects. Models for Pacific herring and Pacific hake could not use Diel as a predictor, because we could only classify fish acoustic backscatter to species for day samples.

fullness occurred at the highest dissolved oxygen levels (80% credible interval = 3.5-5.4 mg/L).

DISCUSSION

Here we used natural spatiotemporal contrast in water quality conditions in Hood Canal, WA, to test specific hypotheses regarding how dissolved oxygen would affect a pelagic food web. We had expected that when dissolved oxygen dropped below biological thresholds, pelagic fish backscatter would decline, feeding intensity on euphausiids would be reduced, and zooplankton would thereby increase through predation release. Overall, these expectations were not borne out by our data and analysis. We failed to detect an effect of dissolved oxygen on most of those processes, and when we did, the effects were often in the opposite direction of our expectations. For instance, zooplankton, if anything, became less abundant while Pacific herring and combined fish became more abundant, and Pacific hake became less abundant, as dissolved oxygen declined below estimated thresholds.

Our expectations were based on numerous sources from the literature, spanning multiple ecosystems and physiological studies. herring were exposed to oxygen levels well below thresholds known to induce behavioral responses in other systems or by other species. Pelagic fish in other systems commonly avoid oxygen levels below 3 mg/L (Klumb et al. 2004, Ludsin et al. 2009) and other fish species in Hood Canal have demonstrated

TABLE 2. Model weights for alternative models fit to feeding metrics for Pacific herring and Pacific hake.

Model	Pacific herring		Pacific hake	
	Fullness	Diet fraction	Fullness	Diet fraction
Base	0.145	0	0.397	0.237
Base + pLarge	0	0.422	0	0
Base + Month	0	0	0.603	0.507
Base + pLarge + Month	0.13	0.578	0	0.256
Base + Dissolved Oxygen	0	0	0	0
Base + pLarge + Dissolved Oxygen	0.725	0	0	0
Base + Month + Dissolved Oxygen	0	0	0	0
Base + pLarge + Month + Dissolved Oxygen	0	0	0	0

Note: pLarge refers to the estimated proportion of sampled Euphausiid biomass that was greater than 10 mm, and Base refers to the combination of Site random effects and Year + Diel fixed effects.

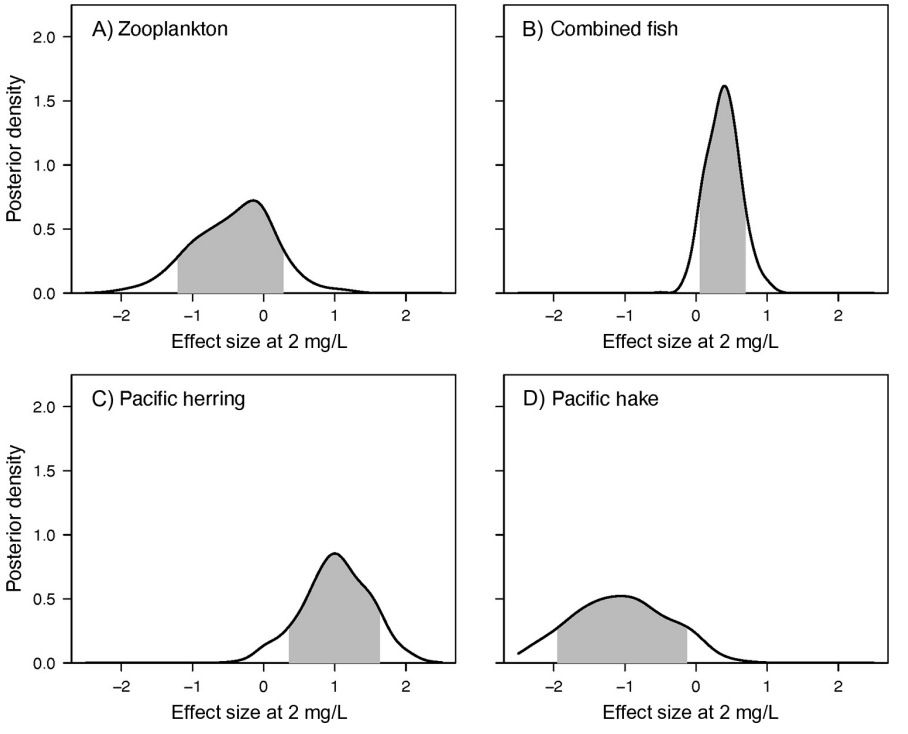

FIG. 5. Posterior probability densities of the estimated effect of dissolved oxygen on acoustic backscatter. Effect sizes refer to the predicted change in response variable, on a $\log_e$ scale, when dissolved oxygen was 2.0 mg/L compared to when oxygen was greater than the estimated threshold value. Values of 0 indicate no effect, negative values imply a decline in the response variable, positive values imply an increase. Shaded area represents the inner 80% credible region.

distributional shifts at dissolved oxygen levels near 2.0 mg/L (Essington and Paulsen 2010). Moreover, Froehlich et al. (2015) observed that Pacific herring in Hood Canal experienced hypoxia-stress, based on increased levels of transcriptional proteins that induce physiological responses (e.g., lowered metabolism, efficient oxygen transfer, use, and storage) that help organisms cope with oxygen limitation. Dommasnes et al. (1994) found that overwintering Atlantic herring avoid areas with dissolved oxygen concentrations near or below 2 mg/L, which correspond to the lowest observed dissolved oxygen concentrations in the present study. Herbert and Steffensen (2006) also found that Atlantic herring increase swim speeds at dissolved oxygen levels <4.5 mg/L, presumably to find more favorable habitat. The estimated decline in Pacific hake backscatter at dissolved oxygen concentrations below 2.6–3.8 was equally surprising, given that this species commonly resides at even lower dissolved oxygen concentrations in coastal oceans (Keller et al. 2010).

Although it is not surprising that there was not high support for models containing dissolved oxygen as a predictor of zooplankton backscatter, it is surprising that the analysis suggested a decline in backscatter in

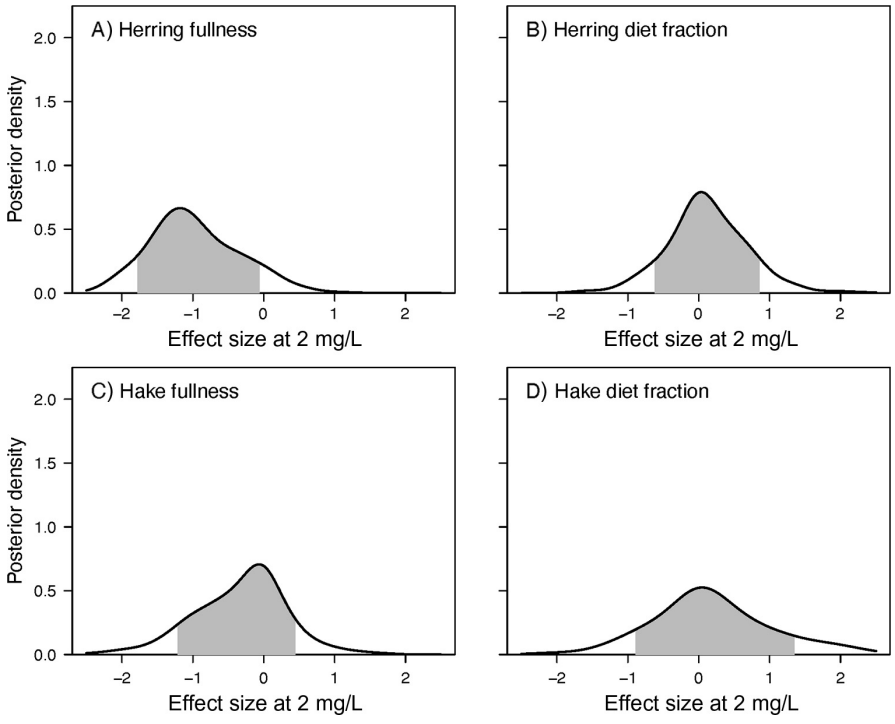

FIG. 6. Posterior probability densities of the estimated effect of dissolved oxygen on feeding metrics. Effect size for fullness refers to the predicted change in response variable, on a $\log_e$ scale, when dissolved oxygen was 2 mg/L compared to when oxygen was greater than the estimated threshold value. Effect size for diet fraction is the predicted change in the log odds ratio. Shaded area represents the inner 80% credible region.

TABLE 3. Estimated threshold dissolved oxygen concentrations (mg/L) and 80% credible intervals, compared to the prior probability distribution.

Response	Median	Lower	Upper
Zooplankton backscatter	3.5	2.4	4.7
Combined fish backscatter	3.0	2.2	4.0
Pacific herring backscatter	3.6	2.5	4.4
Pacific hake backscatter	2.5	2.2	3.3
Pacific herring stomach fullness	4.3	2.8	5.3
Pacific herring diet fraction	2.7	2.1	4.5
Pacific hake stomach fullness	2.8	2.2	4.3
Pacific hake diet fraction	2.9	2.2	4.9
Prior probability	3.5	2.3	5.2

response to declining oxygen levels. Euphausiids are generally recognized to be tolerant of dissolved oxygen levels within the range experienced in Hood Canal during this study (Tremblay and Abele 2016). Two analyses of data from this same study also found little evidence of distributional or demographic effects on euphausiids. Sato et al. (2016) found no evidence that *Euphausia pacifica* exhibited vertical distributional shifts in response to dissolved oxygen, and Li et al. (2019) could not detect a decline in juvenile or adult water column densities indicative of hypoxia-induced mortality.

We cannot state equivocally why our expectations were not met, but we identify plausible explanations that could serve as hypotheses for further study. Because low dissolved oxygen is common in Hood Canal, it is possible that these species may acclimate to commonly experienced oxygen levels via adaptations to gill surface area (Sollid et al. 2003), blood oxygen carrying capacity (Tetens and Lykkeboe 1981), or routine metabolic rate (Mandic et al. 2009). Given that water temperature was generally between 9° and 10°C when dissolved oxygen concentration was lowest (Appendix S1: Fig. S2 and Sato et al. 2016), the relatively cool water temperatures could minimize metabolic demands and increase tolerance to low dissolved oxygen (Pörtner and Knust 2007). Finally, unlike other estuaries where low dissolved oxygen is tied to recent anthropogenic causes, Hood Canal has been subject to seasonal low dissolved oxygen for centuries (Brandenberger et al. 2011) with substantial potential for population adaption (Decker et al. 2003). The recurrent seasonal oxygen depletion may have also shaped the zooplankton and planktivore fish species assemblages, such that only those species that can tolerate low dissolved oxygen concentrations have persisted (Wu 2002).

Alternatively, our findings may represent the challenges of disentangling effects of seasonal hypoxia from other environmental and biological phenology. This

comparative field survey was designed to include high spatial contrasts in oxygen concentrations at two pairs of sites. Such comparative designs are commonly used in environmental impact assessments (Underwood 1992, 1994), yet only via a large-scale experiment where dissolved oxygen was experimentally manipulated could one completely separate phenology and localized site effects from the dissolved oxygen-induced responses (Carpenter et al. 1998). The observed high variance in some of the response variables (e.g., Figs. 3 and 4) also may have diminished power to detect effects in spite of our sampling design (Underwood and Chapman 2003).

Our data and analysis suggest the possibility that low dissolved oxygen strengthened the intensity of predation pressure by Pacific herring on zooplankton, despite our previous findings that spatial overlap during the same sampling period was insensitive to dissolved oxygen finding (Sato et al. 2016). Taking the product of Pacific herring biomass, stomach fullness, and diet fraction as an index of euphausiid consumption intensity, and the ratio of consumption intensity to zooplankton backscatter as an index of relative predation intensity, we found that the posterior density of predation intensity had a median of 1.08, though the distribution was broad (80% credibility interval: −0.4 to 2.5). Thus, the integrative measure of predation intensity gives weak support to the hypothesis that predation intensity increased when dissolved oxygen declined to its lowest levels, near 2 mg/L. Additional analysis to enhance the statistical power is needed to better quantify how hypoxia altered this predator–prey linkage, and more information is needed on the relative predation intensity of Pacific herring and Pacific hake on euphausiids.

Our findings illustrate the value of in situ observations of ecological processes to support those suggested by laboratory experiments, models, or proxies. For instance, spatial overlap between predators and prey is commonly thought to be a proxy for energy transfer and trophic connectivity, such that changes in spatial overlap are believed to change energy fluxes (Taylor and Rand 2003, Ludsin et al. 2009, Vanderploeg et al. 2009, Zhang et al. 2009). In our system, vertical spatial overlap between predators and prey was maintained during periods when dissolved oxygen levels were near or below 2.0 mg/L (Sato et al. 2016). Yet, the present study that simultaneously examined predator and prey densities, predator feeding rates, and diet composition revealed evidence for strengthened predator–prey linkage between herring and their euphausiid prey. Increased use of comparative analyses with synoptic sampling of systemic properties (e.g., energy flow among food web compartments) will strengthen our ability to predict consequences of future oxygen depletion in coastal ecosystems worldwide.

Acknowledgments

We thank the crew of the R/V Clifford Barnes and R/V Centennial, Lilia Bannister, Sarah Tekola, Jen Nomura, BethElLee Hermann, Amanda Winans, and Rebecca Stiling who assisted with fieldwork and/or lab processing of samples. We also thank two reviewers whose comments improved the quality of the manuscript. This work was supported by the National Science Foundation OCE-1154648AM001. All data are available in BCO-DMO, the data repository of the Biological and Chemical Data Management Office, and data, R, and Stan code are available on Zenodo; see the Data Availability section for direct links.

Literature Cited

Anderson, D. R., K. P. Burnham, and W. L. Thompson. 2000. Null hypothesis testing: Problems, prevalence, and an alternative. Journal of Wildlife Management 64:912–923.

Babson, A. L., M. Kawase, and P. MacCready. 2006. Seasonal and interannual variability in the circulation of Puget Sound, Washington: A box model study. Atmosphere-Ocean 44:29–45.

Boyd, C. M., S. L. Smith, and T. J. Cowles. 1980. Grazing patterns of copepods in the upwelling system off Peru. Limnology and Oceanography 25:583–596.

Brandenberger, J. M., P. Louchouarn, and E. A. Crecelius. 2011. Natural and post-urbanization signatures of hypoxia in two basins of puget sound: historical reconstruction of redox sensitive metals and organic matter inputs. Aquatic Geochemistry 17:645–670.

Breitburg, D. 1992. Episodic hypoxia in Chesapeake Bay: Interacting effects of recruitment, behavior, and physical disturbance. Ecological Monographs 62:525–546.

Breitburg, D., et al. 2018. Declining oxygen in the global ocean and coastal waters. Science 359(6371):eaam7240.

Buckley, L. B., M. C. Urban, M. J. Angilletta, L. G. Crozier, L. J. Rissler, and M. W. Sears. 2010. Can mechanism inform species' distribution models? Ecology Letters 13:1041–1054.

Carpenter, J. H. 1965. The accuracy of the winkler method for dissolved oxygen analysis1. Limnology and Oceanography 10:135–140.

Carpenter, S. R., J. T. Cole, T. E. Essington, J. R. Hodgson, J. N. Houser, J. F. Kitchell, and M. L. Pace. 1998. Evaluating alternative explanations in ecosystem experiments. Ecosystems 1:335–344.

Chueng, W. W. L., J. L. Sarmiento, J. A. Dunne, T. L. Frölicher, V. W. Y. Lam, M. L. D. Palomares, R. Watson, and D. Pauly. 2013. Shrinking of fishes exacerbates impacts of global ocean changes on marine ecosystems. Nature Climate Change 3:254–258.

Clark, J. S., et al. 2001. Ecological forecasts: an emerging imperative. Science 293:657–660.

Craig, J. K., and L. B. Crowder. 2005. Hypoxia-induced habitat shifts and energetic consequences in Atlantic croaker and brown shrimp on the Gulf of Mexico shelf. Marine Ecology Progress Series 294:79–94.

Davis, C. S., and P. H. Wiebe. 1985. Macrozooplankton biomass in a warm-core Gulf Stream ring: Time series changes in size structure, taxonomic composition, and vertical distribution. Journal of Geophysical Research: Oceans 90:8871–8884.

Decker, M. B., D. L. Breitburg, and N. H. Marcus. 2003. Geographical differences in behavioral responses to hypoxia: Local adaptation to an anthropogenic stressor? Ecological Applications 13:1104–1109.

Decker, M. B., D. L. Breitburg, and J. E. Purcell. 2004. Effects of low dissolved oxygen on zooplankton predation by the ctenophore *Mnemiopsis leidyi*. Marine Ecology Progress Series 280:163–172.

Deutsch, C., A. Ferrel, B. Seibel, H. O. Portner, and R. B. Huey. 2015. Climate change tightens a metabolic constraint on marine habitats. Science 348:1132–1135.

Diaz, R. J., and R. Rosenberg. 2008. Spreading dead zones and consequences for marine ecosystems. Science 321:926–929.

Dommasnes, A., F. Rey, and I. Røttingen. 1994. Reduced oxygen concentrations in herring wintering areas. ICES Journal of Marine Science 51:63–69.

Domenici, P., C. Lefrançois, and A. Shingles. 2007. Hypoxia and the antipredator behaviours of fishes. Philosophical Transactions of the Royal Society B 362:2105–2121.

Eby, L. A., and L. B. Crowder. 2002. Hypoxia-based habitat compression in the Neuse River Estuary: context-dependent shifts in behavioral avoidance thresholds. Canadian Journal of Fisheries and Aquatic Sciences 59:952–965.

Ekau, W., H. Auel, H.-O. Pörtner, and D. Gilbert. 2010. Impacts of hypoxia on the structure and processes in pelagic communities (zooplankton, macro-invertebrates and fish). Biogeosciences 7:1669–1699.

Essington, T. E., and C. E. Paulsen. 2010. Quantifying hypoxia impacts on an estuarine demersal community using a hierarchical ensemble approach. Ecosystems 13:1035–1048.

Flyvbjerg, H., and H. G. Petersen. 1989. Error estimates on averages of correlated data. Journal of Chemical Physics 91:461–466.

Froehlich, H. E., S. B. Roberts, and T. E. Essington. 2015. Evaluating hypoxia-inducible factor-1alpha mRNA expression in a pelagic fish, Pacific herring Clupea pallasii, as a biomarker for hypoxia exposure. Comparative Biochemistry and Physiology Part A Molecular Integrative Physiology 189:58–66.

Fry, F. E. J. 1971. The effect of environmental factors on the physiology of fish. Fish Physiology 6:1–98.

Gelman, A. 2006. Prior distributions for variance parameters in hierarchical models (comment on article by Browne and Draper). Bayesian Analysis 1:515–534.

Gelman, A., and D. B. Rubin. 1992. Inference from iterative simulation using multiple sequences. Statistical Science 7:457–511.

Guzzo, M. M., P. J. Blanchfield, and M. D. Rennie. 2017. Behavioral responses to annual temperature variation alter the dominant energy pathway, growth, and condition of a cold-water predator. Proceedings of the National Academy of Sciences USA 114:9912–9917.

Harley, C. D. G., A. R. Hughes, K. M. Hultgren, B. G. Miner, C. J. B. Sorte, C. S. Thornber, L. F. Rodriguez, L. Tomanek, and S. L. Williams. 2006. The impacts of climate change in coastal marine systems. Ecology Letters 9:228–241.

Herbert, N. A., and J. F. Steffensen. 2006. Hypoxia increases the behavioural activity of schooling herring: a response to physiological stress or respiratory distress? Marine Biology 149:1217–1225.

Hilborn, R., and M. Mangel. 1997. The ecological detective. Princeton University Press, Princeton, New Jersey, USA.

Hoffman, M. D., and A. Gelman. 2014. The No-U-Turn sampler: adaptively setting path lengths in Hamiltonian Monte Carlo. Journal of Machine Learning Research 15:1593–1623.

Keister, J. E., E. D. Houde, and D. L. Breitburg. 2000. Effects of bottom-layer hypoxia on abundances and depth distributions of organisms in Patuxent River, Chesapeake Bay. Marine Ecology Progress Series 205:43–59.

Keister, J. E., and L. B. Tuttle. 2013. Effects of bottom-layer hypoxia on spatial distributions and community structure of mesozooplankton in a sub-estuary of Puget Sound, Washington, U.S.A. Limnology and Oceanography 58:667–680.

Keister, J. E., A. K. Winans, and B. Herrmann. 2020. Zooplankton community response to seasonal hypoxia: A test of three hypotheses. Diversity 12:21.

Keller, A. A., V. Simon, F. Chan, W. W. Wakefield, M. E. Clarke, J. A. Barth, D. Kamikawa, and E. L. Fruh. 2010. Demersal fish and invertebrate biomass in relation to an offshore hypoxic zone along the US West Coast. Fisheries Oceanography 19:76–87.

Klumb, R. A., K. L. Bunch, E. L. Mills, L. G. Rudstam, G. Brown, C. Knauf, R. Burton, and F. Arrhenius. 2004. Establishment of a metalimnetic oxygen refuge for zooplankton in a Productive Lake Ontario embayment. Ecological Applications 14:113–131.

Kolesar, S. E., D. L. Breitburg, J. E. Purcell, and M. B. Decker. 2010. Effects of hypoxia on *Mnemiopsis leidyi*, ichthyoplankton and copepods: clearance rates and vertical habitat overlap. Marine Ecology Progress Series 411:173–188.

Koslow, J. A., R. Goericke, A. Lara-Lopez, and W. Watson. 2011. Impact of declining intermediate-water oxygen on deepwater fishes in the California Current. Marine Ecology Progress Series 436:207–218.

Lavaniegos, B. E., and M. D. Ohman. 2007. Coherence of long-term variations of zooplankton in two sectors of the California Current System. Progress in Oceanography 75:42–69.

Lavery, A. C., P. H. Wiebe, T. K. Stanton, G. L. Lawson, M. C. Benfield, and N. Copley. 2007. Determining dominant scatterers of sound in mixed zooplankton populations. Journal of the Acoustical Society of America 122:3304–3326.

Levin, S. A. 1998. Ecosystems and the biosphere as complex adaptive systems. Ecosystems 1:431–436.

Li, L., J. E. Keister, T. E. Essington, and J. Newton. 2019. Vertical distributions and abundances of life stages of the euphausiid *Euphausia pacifica* in relation to oxygen and temperature in a seasonally hypoxic fjord. Journal of Plankton Research 41:188–202.

Little, W. S., and N. J. Copley. 2003. WHOI silhouette digitizer version 1.0 User's guide. Technical Report, Woods Hole Oceanographic Institute.

Ludsin, S. A., X. S. Zhang, S. B. Brandt, M. R. Roman, W. C. Boicourt, D. M. Mason, and M. Costantini. 2009. Hypoxia-avoidance by planktivorous fish in Chesapeake Bay: Implications for food web interactions and fish recruitment. Journal of Experimental Marine Biology and Ecology 381:S121–S131.

Maclennan, D. N., P. G. Fernandes, and J. Dalen. 2002. A consistent approach to definitions and symbols in fisheries acoustics. ICES Journal of Marine Science 59:365–369.

Mandic, M., A. E. Todgham, and J. G. Richards. 2009. Mechanisms and evolution of hypoxia tolerance in fish. Proceedings of the Royal Society B 276:735–744.

Mauchline, J. 1980. Measurement of body length of Euphausia superba Dana. BIOMASS Handbook No. 4, SCAR/SCOR/IABO/ACMRR:4–9.

Merila, J., and A. P. Hendry. 2014. Climate change, adaptation, and phenotypic plasticity: the problem and the evidence. Evolutionary Applications 7:1–14.

Moriarty, P. E., T. E. Essington, and E. J. Ward. 2017. A novel method to estimate prey contributions to predator diets. Canadian Journal of Fisheries and Aquatic Sciences 74:168–177.

Nestlerode, J. A., and R. J. Diaz. 1998. Effects of periodic environmental hypoxia on predation of a tethered polychaete, Glycera Americana: implications for trophic dynamics. Marine Ecology Progress Series 172:185–195.

Newton, J., C. Bassin, A. Devol, M. Kawase, W. Reuf, M. Warner, D. Hannafious, and R. Rose. 2007. Hypoxia in Hood Canal: An overview of status and contributing factors. Page 11 *in* Proceedings of the Georgia Basin Puget Sound Research Conference. University of Washington School of Engineering, Seattle, Washington, USA.

Oschlies, A., P. Brandt, L. Stramma, and S. Schmidtko. 2018. Drivers and mechanisms of ocean deoxygenation. Nature Geoscience 11:467.

Parker-Stetter, J. L., and J. K. Horne. 2009. Nekton distribution and midwater hypoxia: a seasonal, diel prey refuge? Estuarine Coastal and Shelf Science 81:13–18.
Pichavant, K., J. Person-Le-Ruyet, N. L. Bayon, A. Severe, A. L. Roux, and G. Boeuf. 2001. Comparative effects of long-term hypoxia on growth, feeding and oxygen consumption in juvenile turbot and European sea bass. Journal of Fish Biology 59:875–883.
Pierson, J. J., M. R. Roman, D. G. Kimmel, W. C. Boicourt, and X. S. Zhang. 2009. Quantifying changes in the vertical distribution of mesozooplankton in response to hypoxic bottom waters. Journal of Experimental Marine Biology and Ecology 381:S74–S79.
Pihl, L., S. P. Baden, and R. J. Diaz. 1991. Effects of periodic hypoxia on distribution of demersal fish and crustaceans. Marine Biology 108:349–360.
Pollock, M. S., L. M. J. Clarke, and M. G. Dube. 2007. The effects of hypoxia on fishes: from ecological relevance to physiological effects. Environmental Reviews 15:1–14.
Pörtner, H. O., and R. Knust. 2007. Climate change affects marine fishes through the oxygen limitation of thermal tolerance. Science 315:95–96.
R Development Core Team. 2017. R: A language and environment for statistical computing. R Development Core Team, Vienna, Austria.
Roman, M. R., S. B. Brandt, E. D. Houde, and J. J. Pierson. 2019. Interactive effects of hypoxia and temperature on coastal pelagic zooplankton and fish. Frontiers in Marine Science 6:18.
Sato, M., J. K. Horne, S. L. Parker-Stetter, T. E. Essington, J. E. Keister, P. E. Moriarty, L. Li, and J. Newton. 2016. Impacts of moderate hypoxia on fish and zooplankton prey distributions in a coastal fjord. Marine Ecology Progress Series 560:57–72.
Sato, M., J. K. Horne, S. L. Parker-Stetter, and J. E. Keister. 2015. Acoustic classification of coexisting taxa in a coastal ecosystem. Fisheries Research 172:130–136.
Sollid, J., P. D. Angelis, K. Gundersen, and G. E. Nilsson. 2003. Hypoxia induces adaptive and reversible gross morphological changes in crucian carp gills. Journal of Experimental Biology 206:3667–3673.
Stalder, L. C., and N. H. Marcus. 1997. Zooplankton responses to hypoxia: behavioral patterns and survival of three species of calanoid copepods. Marine Biology 127:599–607.
Stan Development Team. 2017. The Stan Core Library, Version 2.17.0. https://mc-stan.org
Stramma, L., G. C. Johnson, J. Sprintall, and V. Mohrholz. 2008. Expanding oxygen-minimum zones in the tropical oceans. Science 320:655–658.
Sutherland, D. A., P. MacCready, N. S. Banas, and L. F. Smedstad. 2011. A model study of the salish sea estuarine circulation. Journal of Physical Oceanography 41:1125–1143.
Taylor, J. C., and P. S. Rand. 2003. Spatial overlap and distribution of anchovies (*Anchoa* spp.) and copepods in a shallow stratified estuary. Aquatic Living Resources 16:191–196.
Tetens, V., and G. Lykkeboe. 1981. Blood respiratory properties of rainbow trout, *Salmo gairdneri*: Responses to hypoxia acclimation and anoxic incubation of blood in vitro. Journal of Comparative Physiology 145:117–125.
Tremblay, N., and D. Abele. 2016. Response of three krill species to hypoxia and warming: an experimental approach to oxygen minimum zones expansion in coastal ecosystems. Marine Ecology 37:179–199.
Underwood, A. J. 1992. Beyond BACI—The detection of environmental impacts on populations in the real, but variable, world. Journal of Experimental Marine Biology and Ecology 161:145–178.
Underwood, A. J. 1994. On beyond BACI: Sampling designs that might reliably detect environmental disturbances. Ecological Applications 4:4–15.
Underwood, A. J., and M. G. Chapman. 2003. Power, precaution, type II error and sampling design in assessment of environmental impacts. Journal of Experimental Marine Biology and Ecology 296:49–70.
Vanderploeg, H. A., S. A. Ludsin, S. A. Ruberg, T. O. Hook, S. A. Pothoven, S. B. Brandt, G. A. Lang, J. R. Liebig, and J. F. Cavaletto. 2009. Hypoxia affects spatial distributions and overlap of pelagic fish, zooplankton, and phytoplankton in Lake Erie. Journal of Experimental Marine Biology and Ecology 381:S92–S107.
Vaquer-Sunyer, R., and C. M. Duarte. 2008. Thresholds of hypoxia for marine biodiversity. Proceedings of the National Academy of Sciences USA 105:15452–15457.
Vehtari, A., J. Gabry, M. Magnussen, Y. Yao, A. Gelman. 2019. loo: efficient leave-one-out cross-validation and WAIC for Bayesian Models. R package version 2.2.0. https://mc-stan.org/loo
Vehtari, A., A. Gelman, and J. Gabry. 2017. Practical Bayesian model evaluation using leave-one-out cross-validation and WAIC. Statistics and Computing 27:1413–1432.
Walker, B., C. S. Holling, S. R. Carpenter, and A. Kinzig. 2004. Resilience, adaptability and transformability in social–ecological systems. Ecology and Society 9:5. [online] http://www.ecologyandsociety.org/vol9/iss2/art5
Webber, M. K., and J. C. Roff. 1995. Annual biomass and production of the oceanic copepod community off Discovery Bay, Jamaica. Marine Biology 123:481–495.
Williams, R., and D. Robins. 1979. Calorific, ash, carbon and nitrogen content in relation to length and dry weight of *Parathemisto gaudichaudi* (Amphipoda: Hyperiidea) in the North East Atlantic Ocean. Marine Biology 52:247–252.
Wu, R. S. S. 2002. Hypoxia: from molecular responses to ecosystem responses. Marine Pollution Bulletin 45:35–45.
Yao, Y., A. Vehtari, D. Simpson, and A. Gelman. 2018. Using stacking to average bayesian predictive distributions (with Discussion). Bayesian Analysis 13:917–1007.
Zhang, H., S. A. Ludsin, D. M. Mason, A. T. Adamack, S. B. Brandt, X. Zhang, D. G. Kimmel, M. R. Roman, and W. C. Boicourt. 2009. Hypoxia-driven changes in the behavior and spatial distribution of pelagic fish and mesozooplankton in the northern Gulf of Mexico. Journal of Experimental Marine Biology and Ecology 381:S80–S91.

Data Availability

All data are available in BCO-DMO, the data repository of the Biological and Chemical Data Management Office, at https://www.bco-dmo.org/project/557504. Data, R, and Stan code are available on Zenodo: https://doi.org/10.5281/zenodo.3841863

Supporting Information

Additional supporting information may be found online at: http://onlinelibrary.wiley.com/doi/10.1002/eap.2204/full